Available online at www.sciencedirect.com
ScienceDirect
Ceramics International 37 (2011) 1593–1599
CERAMICS INTERNATIONAL
www.elsevier.com/locate/ceramint

Determination of hardness, Young's modulus and fracture toughness of lanthanum tungstates as novel proton conductors

J.J. Roa [a,*], A. Magrasó [b], M. Morales [a], P. Núñez [c], M. Segarra [a]

[a] Faculty of Chemistry, Department of Materials Science and Metallurgical Engineering, University of Barcelona, Martí i Franquès, 1, 08028 Barcelona, Spain
[b] Department of Chemistry, University of Oslo, Centre for Materials Science and Nanotechnology, FERMiO, Gaustadalléen 21, NO-0349 Oslo, Norway
[c] Department of Inorganic Chemistry, University of La Laguna, 38200, La Laguna, Tenerife, Spain

Received 4 January 2011; received in revised form 17 January 2011; accepted 18 January 2011
Available online 25 January 2011

Abstract

Lanthanum tungstate is a promising material to be used as electrolyte in proton conducting fuel cells, or as a mixed proton–electron conducting membrane for hydrogen separation, and its mechanical properties are crucial for these applications. Lanthanum tungstates with a La/W atomic ratio between 4.8 and 6.0 have been investigated at room temperature at micro/nanoindentation range. Lanthanum tungstates exhibit a strain gradient plasticity at the vicinity of the imprints, which implies that the hardness presents an indentation size effect that was corrected using the Nix and Gao approach. The hardness and Young's modulus have therefore been determined to be 8–9 GPa and 130 ± 15 GPa, respectively. The fracture toughness was estimated to be $\sim$2 MPa $m^{1/2}$ for LWO56 using the Palqmvist equation. Both hardness and Young's modulus did not present a significant dependence with neither the sintering temperature nor the composition. The different imprints were visualized by Atomic Force Microscopy.

Keywords: C. Fracture; C. Hardness; C. Mechanical properties; E. Fuel cells; E. Membranes

1. Introduction

Lanthanum tungstates close to the 3:1 La_2O_3–WO_3 molar ratio, and related compositions, are very promising materials for their use as electrolytes in high temperature proton conducting solid oxide fuel cells (PC-SOFCs), or in mixed proton–electron conducting membranes for hydrogen separation [1–4]. They are predominantly proton conductors under wet atmospheres below $\sim$750 °C, with a maximum proton conductivity of $\sim 3 \times 10^{-3}$ S/cm at 800 °C [4]. At high temperatures, these materials are mixed conductors exhibiting n- and p-type electronic conductivity under reducing and oxidising atmospheres, respectively.

Characterization of the mechanical properties, such as Young's modulus (E), hardness (H) and fracture toughness (K_{IC}), is important for evaluating the mechanical performance of materials to be used in practical applications. There are a number of techniques employed for this purpose; such as Vickers indentation or three-point bend tests. In addition, non-conventional techniques have been developed for evaluating the mechanical properties of solid materials, such as high-resolution, depth-sensing indentation (commonly referred as nanoindentation) [5,6]. We have studied the mechanical properties of lanthanum tungstates with this technique because it provides additional information compared to the conventional techniques cited above. For instance, it allows the determination of mechanical properties located on small structural features in the materials, due to its small measurement length scale and quasi-non-destructive nature. Therefore, this technique can be used to measure the local Young's modulus and hardness in different types of materials, ruling out the influence of the macroscopic defects (porosity, cracks, grain size, etc.), which is less straightforward with other more conventional techniques [7]. A Berkovick indenter is generally used in small scale indentation studies as it has the advantage that its pyramidal edges are more easily constructed to meet at a single point compared to a Vickers indenter [7].

According to Magrasó et al. [8], stoichiometric La_6WO_{12} cannot be prepared as pure phase composition at temperatures below 1600 °C, and single phase materials could only be

* Corresponding author.
E-mail address: jjrr_cons@hotmail.com (J.J. Roa).

0272-8842/$36.00
doi:10.1016/j.ceramint.2011.01.002

obtained when the La/W ratio was between 5.3 and 5.7, for a sintering temperature of 1500 °C. Outside this compositional range, segregation of either La_2O_3 (La/W $\geq$ 5.8) or $La_6W_2O_{15}$ (La/W $\leq$ 5.2) were found. Conductivity-wise, compositions with minor La_2O_3 segregation show similar conductivity values as the single phase ones [4,8], but those containing segregation of W-rich phases show a considerable drop in conductivity with increasing content of the secondary phase [8]. Structure-wise, the composition with a La/W nominal atomic ratio of 5.6 (LWO56) could be described as a face-centred fluorite-type structure with a disordered inherently deficient oxygen sublattice, and the formula unit can be written as $La_{6.63}W_{1.17}O_{13.43}$ ($Z = 4$; calculated density = 6.395 g/cm^3) [8]. One of the aims of the present work is to determine whether compositional differences, the presence of segregations or the sintering temperature influence the mechanical properties of the materials. Additionally, and to the best of our knowledge, this is the first time that the mechanical properties of these lanthanum tungstates have ever been reported. The mechanical properties of lanthanum tungstate reported here will also be compared to other well-known fluorite-type structures used as electrolytes in classical SOFCs, such as yttria stabilised zirconia (YSZ) or gadolinium doped ceria (GDC) [9], and other high temperature proton conductors, such as $LaNbO_4$ [10].

The purpose of this work is to determine the mechanical properties of lanthanum tungstates with a La/W atomic ratio between 4.8 and 6 by using micro- and nano-indentation techniques. The indentation size effect (ISE) was determined and ruled out for the final given properties. The effect of sintering temperature and composition on the mechanical properties is discussed.

2. Experimental

2.1. Sample preparation

For the sake of simplicity, the compositions will be hereafter labelled as LWO*x*, where *x* represents the nominal La/W ratio multiplied by 10. Polycrystalline powders of lanthanum tungstates with a La/W cation ratio between 4.8 (LWO48) and 6.0 (LWO60) were prepared by freeze-drying synthesis, as described in Ref. [8]. Calcination of each composition was performed at 1000 °C for 5 h, and sintering was held between 1350 and 1600 °C for 2 h. Single phase materials were only obtained when the La/W cation ratio layed between 5.3 and 5.7; compositions with higher lanthanum content revealed segregations of La_2O_3, and higher tungsten content showed more $La_6W_2O_{15}$ [8]. Prior to nanoindentation, the sintered specimens were polished with diamond suspensions of 30, 6, 3, 1, 1/4 μm and colloidal silica.

2.2. Mechanical characterization

2.2.1. Microindentation tests

Microindentation tests were performed on the polished longitudinal section using an ISOSCAN OD Galileo Durometer. This study was carried out using a Vickers diamond tip indenter. The maximum applied load was 5000 mN. Fifteen indentations were made on each sample, and the results were averaged.

2.2.2. Nanoindentation tests

Nanoindentation tests were performed on the polished longitudinal sections with a Nanoindenter® XP System (Agilent Technologies) equipped with Test Works 4 Professional level software. Nanoindentations were performed by a three-sided pyramid Berkovich diamond indenter. The penetration depth was continuously monitored at a constant deformation velocity of 0.05 s^{-1}, and load-time history of indentation was recorded. The Berkovich tip employed during the indentation process was calibrated against a fused silica standard. Fifty indentations were made on each sample, and the results were averaged. The mechanical properties have been studied at different penetration depths (from 150 nm to 2000 nm) using the Oliver and Pharr equations [5,6,11] and the fracture toughness has been calculated from indentations at 2000 nm.

The residual imprints of each sample were observed by AFM (Digital Instruments Multimode) in contact mode, and the images were treated using WSxM software [12].

2.3. Fracture mechanisms

A critical mechanical parameter in brittle materials is the fracture toughness K_{IC} [13], which characterizes its resistance against crack propagation. Fracture toughness can be estimated from the length of the cracks nucleated at the corners of the residual imprint, a method known as indentation microfracture. Several expressions have been proposed to determine K_{IC} depending on the tip indenter geometry and crack morphology (radial, half penny or Palqmvist). For radial cracks, the most widely employed expression is [14]:

$$K_{IC} = \alpha \left(\frac{E}{H}\right)^{1/2} \left(\frac{P}{c^{3/2}}\right) \quad (1)$$

where α is an (dimensionless) empirical constant depending on the indenter geometry (α = 0016 for pyramidal tips), P (in mN) is the peak indentation load, c (in μm) is the length of the radial cracks. For Palmqvist cracks, the following equation applies [15]:

$$K_{IC} = \chi_v \left(\frac{a}{l}\right)^{1/2} \left(\frac{E}{H}\right)^{2/3} \left(\frac{P}{c^{3/2}}\right) \quad (2)$$

where χ_v is 0.016 for a Berkovich tip indenter, a (μm) is the length from the centre of the imprint until one of the corners, and l (μm) is the crack length. The applicability of the different expressions for indentation microfracture test performed with and Berkovich indenters has been extensively discussed in [16,17].

2.4. Indentation size effect models

In order to observe the indentation size effect (ISE) contribution, the hardness has been obtained at different penetration depths (from 150 nm up to 2000 nm) using a Nanoindenter. In addition, several imprints have been performed using a Microindenter at 5000 mN of applied load, which leads to penetration depths of around 4000 nm.

Although numerous mechanistic approaches have been proposed to explain this experimentally observed phenomenon [17], the most widely used model to explain the indentation size effect was developed by Nix and Gao. This model is based on the concept that dislocations are geometrically necessary. Dislocations must be present near the indentation to accommodate the volume of material displaced by the indenter at the surface. In the Nix and Gao model, the indenter is assumed to be a rigid cone whose self-similar geometry is defined by the angle, θ, between the indenter and the non-deformed surface. The hardness value can accordingly be extracted from the following equation:

$$H^2 = H_o^2\left(1 + \frac{h^*}{h}\right) \quad (3)$$

where H is the hardness for a given depth of indentation, h (nm), H_o (GPa) is the hardness at the limit of infinite depth and h^* (nm) is a characteristic length that depends on the shape of the indenter, the shear modulus and H_o. This expression will thus be used to extract the hardness of the studied material.

3. Results and discussion

3.1. Hardness and Young's modulus determination

Fig. 1 shows the evolution of both hardness and Young's modulus at different penetration depths for a representative sample. On the one hand, the Young's modulus does not vary significantly with penetration depth; remains essentially constant. Also, it can be seen from Table 1 that there is no clear dependency of the Young's Modulus with sintering temperature nor composition, and for all tungstates studied here. On the other hand, the hardness does present an indentation size effect, i.e. the apparent hardness is higher at low penetration depths. This phenomenon is known and has been reported for other ceramic materials [18], and the hardness can determined for each composition using the Nix and Gao model. As way of example, Fig. 2 displays the variation of H^2 versus $1/h$ for one composition (LWO48) and shows that the present data fits well to this model, with the exception for the lowest penetration depth (150 nm). This may indicate that for this penetration depth, the size of the indent is in the order of surface defects (e.g. porosity, etc.) so that the model does not apply and this point should be disregarded. This behaviour is representative for all compositions studied here. Such a result attests that the ISE is not an artefact due to the indenter shape calibration. Then, one may also observe from Table 1 that the hardness determined at 2000 nm of penetration depth (Oliver and Pharr) and the hardness extracted after the Nix and Gao correction are very similar. This implies that the ISE at 2000 nm penetration depth is relatively small and the hardness at this penetration depth can be used as a good approximation to the hardness at the limit of infinite depth.

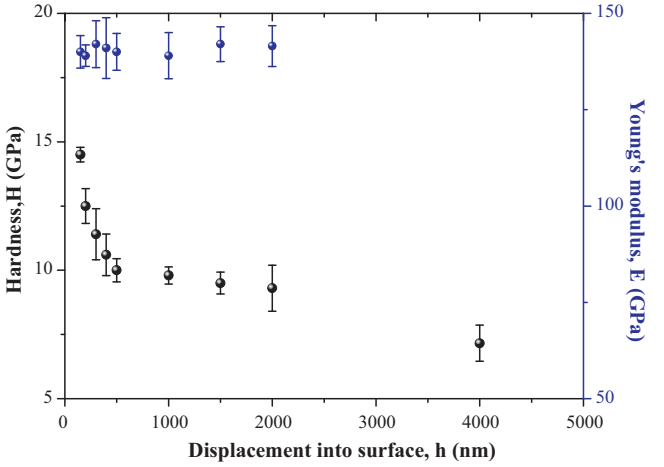

Fig. 1. Hardness and Young's modulus evolution at different penetration depths for LWO48 sintered at 1500 °C.

The difference among all these lanthanum tungstates is the chemical composition, the grain size and the presence of impurities, as summarized in Table 1. A closer look to these values leads us to point out that for the specimens sintered at 1500 °C, or above, H_0 and $H_{\text{Oliver and Pharr}}$ are in very good agreement (below ~5% difference). When the sintering

Table 1
Hardness value (H_o) and Young's modulus for different LWO composition and sintering temperatures obtained using the Nix and Gao [17] equation and Oliver and Pharr approach [5], respectively.

Composition	$T_{sintering}$ (°C)	Grain size (μm)	Relative density (%)	H_o (GPa)	$H_{\text{Oliver and Pharr}}$ (GPa)	E (GPa)	Phase
LWO48	1500	3–10	97	8.5 ± 0.3	8.4 ± 0.8	142 ± 5	Fluorite + $La_6W_2O_{15}$
LWO54	1400	1–3	91	7.9 ± 0.3	8.9 ± 0.9	123 ± 4	Fluorite single phase
	1500	3–10	94	8.5 ± 0.1	8.5 ± 0.7	122 ± 5	Fluorite single phase
LWO56	1400	1–3	93	8.8 ± 0.3	9.3 ± 0.9	141 ± 5	Fluorite + La_2O_3
	1500	3–10	95	8.6 ± 0.3	8.6 ± 0.7	137 ± 3	Fluorite single phase
LWO57	1350	0.8–2	90	8.6 ± 0.4	8.5 ± 0.4	133 ± 2	Fluorite + La_2O_3
LWO58	1550	6–20	98	8.9 ± 0.1	8.4 ± 0.3	114 ± 3	Fluorite single phase
LWO60	1400	1–3	91	–	8.9 ± 0.5	136 ± 8	Fluorite + La_2O_3
	1600	10–30	96	8.3 ± 0.1	8.6 ± 0.6	134 ± 5	Fluorite + La_2O_3

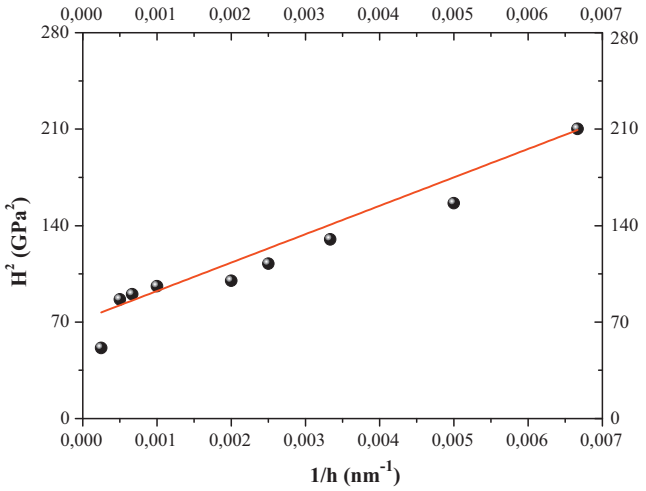

Fig. 2. Representation of H^2 versus $1/h$ for LWO48 at 1500 °C, linear regression corresponds to that described in Eq. (3).

temperature is 1400 °C, or below, the hardness calculated from the Oliver and Pharr approach at 2000 nm penetration depth is somewhat higher (between ∼5 and 10%) than the hardness at the limit of infinite depth, although the difference may still be considered acceptable within error bars. This small difference could be ascribed to the presence of a higher degree of porosity and/or the presence of more impurities, such as La_2O_3 in the La-richer compositions [8].

Representative SEM micrographs of different compositions annealed at different temperatures are presented in Fig. 3. One can observe that the grain size is strongly dependent on final annealing temperature. As already reported by Magrasó et al. [8], the average grain size increases from 1–3 μm (1400 °C), 3–10 μm (1500 °C) to 10–30 μm (1600 °C). The densification properties and variation of particle size of the different LWO compositions do not differ significantly, even those containing segregation of either La- or W-rich phases. This is also shown in Table 1. Arrows in Fig. 3a point at secondary phases, probably corresponding to La_2O_3 in LWO60. This specimen was polished and annealed 100 °C below the sintering temperature so that the impurities would show up on the surface. Tungsten-rich segregations corresponding to $La_6W_2O_{15}$ in low La/W ratios are more easily detected by SEM (see LWO50, Fig. 3c). LWO56 annealed at 1500 °C shows no segregation of phases, in accordance with Ref. [8]. These images exhibit a low pore density in the longitudinal (Fig. 3) and transversal direction (see Fig. 4). This is also accordance with the densities reported in Ref. [8]. All the samples studied here present relative densities of, at least, 90%, which minimizes the ISE. We should highlight here that size of impurities and pores are much smaller than the contact area, in particular, at high penetration depths, and it is therefore expected that the influence of these in the mechanical properties is not very big. The present set of data confirms this.

Another relevant result is that both hardness and Young's modulus do not seem to vary significantly with sintering temperature. This first indicates that there is no appreciable size effect during the first stages of contact between the indenter and the specimen for this penetration depth. As shown in Fig. 1, the

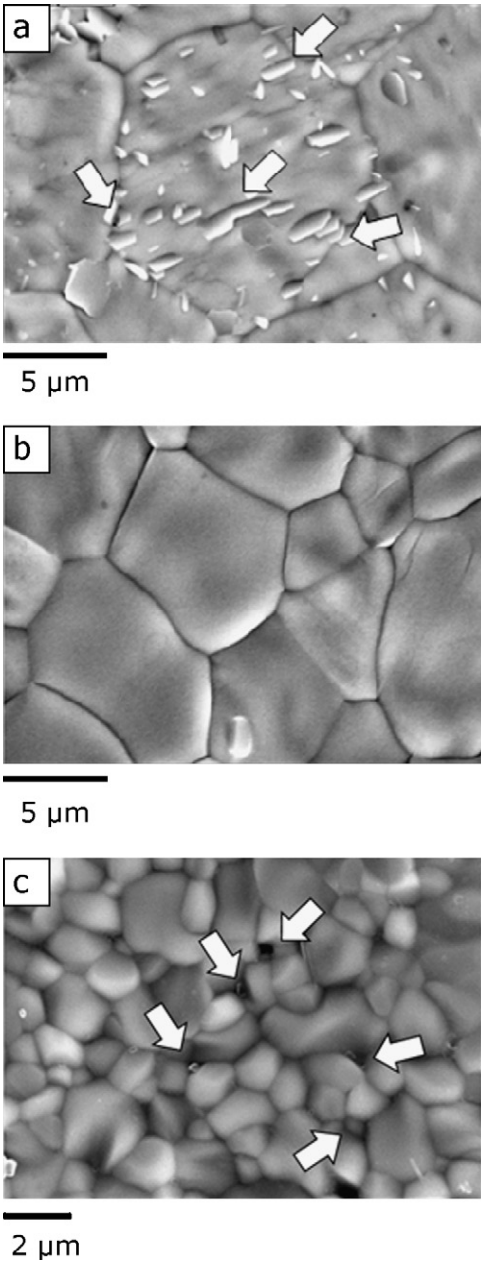

Fig. 3. SEM micrographs taken from the surface of (a) LWO60, $T = 1600$ °C, (b) LWO56, $T = 1500$ °C, and (c) LWO50, $T = 1400$ °C.

Hardness and Young's modulus do not follow a clear trend with sintering temperature between 1350 and 1600 °C, one may speculate that this occurs because the density of the specimens at this temperature range is quite high, ≥90% of the relative density. Then, it also follows that an increase of the grain size from ∼1 (1350 °C) to ∼30 μm (1600 °C) does not influence neither the hardness nor the Young's modulus. Finally, there seems to be no dependency of the mechanical properties with composition or sintering temperature, the values are the same within error bars. LWO57, LWO56 and LWO54 are single phase materials at 1500 °C, but LWO57 and LWO56 present some La_2O_3, at 1400 °C, and below. LWO58 is single phase at 1550 °C and above, and LWO60 have some minor segregation of La_2O_3, even after annealing at 1600 °C, and the lower the

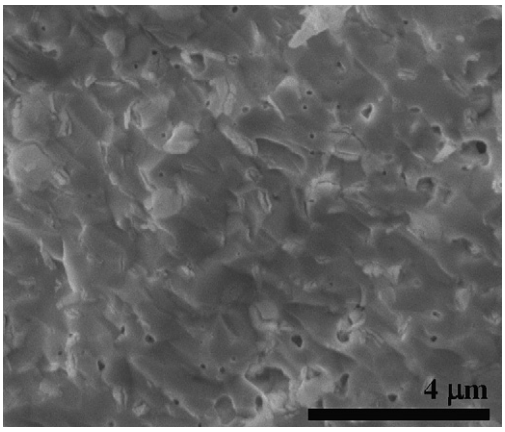

Fig. 4. SEM micrograph of the cross section view after fracture of LWO54 sintered at 1500 °C.

sintering temperature, the more segregation it shows. LWO48 has some $La_6W_2O_{15}$ [8]. This means that the mechanical properties reported here do not vary due to the presence of a minor amount of impurities. This further implies that non-stoichiometry in this material, within the studied compositional range, does not alter the mechanical properties significantly. This eases the applicability of the material and the fabrication of this composition(s) without altering its final mechanical performance within a certain compositional range.

Fig. 5 shows AFM images of a typical residual array nanoindentation imprints performed at 2000 nm of penetration depth. In general, it can be observed that the nanoindentations are clean and mostly show normal fracture mechanisms for brittle materials. Porosity is distributed homogeneously at the surface, and some reduction of the pore density is apparent after annealing at higher temperatures. The mechanical properties of lanthanum tungstate do not vary with sintering temperature probably because the pore size is much smaller than the residual contact area, as observed in the micrographs. We should still mention that the presence of porosity may help to partially dissipate some energy, or deform the sample in the elastic regime, which would lead to a slight underestimation of the hardness values. This effect is however thought to be minimal, since there is no clear variation of the hardness with sintering temperature, and the surface defects (pores, etc.) are much smaller than the contact area, which is in turn well defined judged from the AFM images. We may therefore suggest that the values reported here mainly represent the material's intrinsic properties. The residual nanoimprints in Fig. 5a exhibit radial cracks of few microns (from 0.2 to 0.5 μm) at the corners, which is usual in brittle materials. When a diamond indenter penetrates into the sample, it induces a compressive state to the material. During the indentation process, the tip withdraws, and when the generated stress field is relaxed produces radial cracks at the corners of the residual imprints, see the scheme in Fig. 6 for clarity.

We therefore conclude that the hardness after correction of the ISE is 7.9–8.9 GPa, and slightly higher when using the Oliver and Pharr approach (8.4–9.3 GPa). This means that the hardness for all compositions is roughly between 8 and 9 GPa. The Young's modulus (∼130 ± 15 GPa) does not seem to vary significantly neither with composition nor with sintering temperature.

There are no reported mechanical properties for this material that can be compared with, but lanthanum tungstate may be compared with other fluorite-type structures and proton

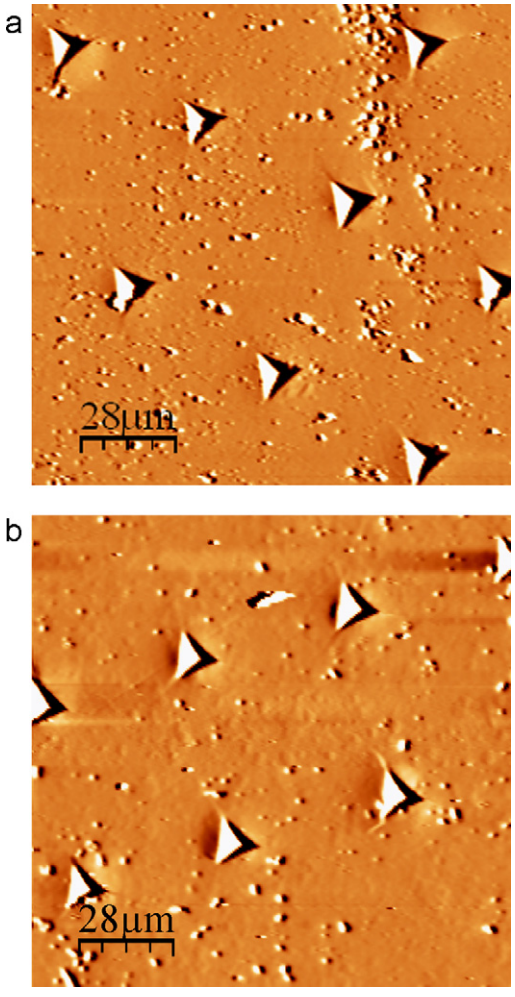

Fig. 5. AFM micrographs of nanohardness imprints at 2000 nm the penetration depth for (a) LWO56 and $T_{sintering}$ = 1400 °C. (b) LWO48 and $T_{sintering}$ = 1500 °C.

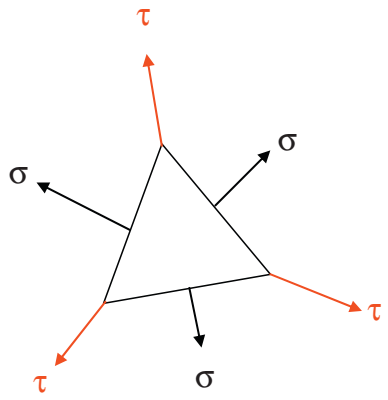

Fig. 6. Scheme of the radial cracks generation during the indentation process.

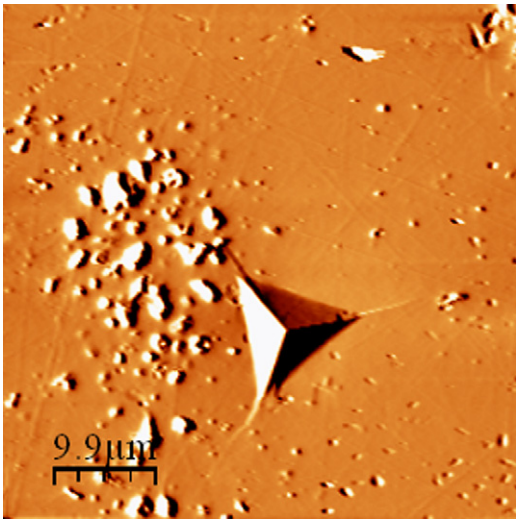

Fig. 7. AFM micrographs of residual nanoindentation imprints developed at 2000 nm of penetration depth for on LWO56 and $T_{sintering}$ = 1400 °C.

conducting materials used as electrolytes in SOFCs or proton conducting SOFCs, respectively. The hardness for GDC and the lanthanum tungstates reported here are approximately the same, while the Young's modulus is lower for LWO compared to GDC: from 180 to 200 GPa depending on the gadolinia doping concentration [9]. YSZ is harder (H = 12.4–13.5 GPa) and presents a higher Young's modulus (200–220 GPa), which is the highest among of all SOFC electrolytes [19]. Acceptor-doped $LaNbO_4$, a recently proposed material as electrolyte for proton conducting fuel cells [10], exhibits lower hardness (∼3 GPa or ∼6 GPa, depending on the dopant concentration and/or grain size [20]) than lanthanum tungstate (∼8–9 GPa). One may overall conclude that lanthanum tungstate presents sufficient mechanical properties for applications as electrolyte in proton conducting fuel cells and/or gas separation membranes.

3.2. Fracture mechanisms

Fig. 7 shows typical AFM micrographs where radial cracks can be observed at the corners of the imprint. All of them show the sink-in effect, typically found in elastic and brittle materials [21]. This effect is an elastic displacement of the surface at the contact perimeter, and could lead to an overestimation of the contact area, and thus an underestimation of the hardness. However, this effect is minimised after calibration with fused silica, and this has been taken into account in the present study.

From the imprints that present radial cracks, the fracture toughness can be estimated. This was calculated for LWO56 sintered at 1400 and 1500 °C, and summarized in Table 2. Other compositions presented porosity surrounding the residual imprint or several fracture mechanisms which were activated due to tensile stresses extended beneath the residual imprint, and therefore K_{IC} could not be obtained by indentation microfracture [22].

Although fracture toughness could only be determined for these two specimens, the measurements seem to indicate that the fracture toughness does not differ significantly with sintering temperature (grain size) between 1400 and 1500 °C for this particular composition, although more experiments should be performed to corroborate this. When comparing these values with other materials, fracture toughness for LWO56 is higher than GDC values reported by Sato et al. [23] (1.2–1.3 MPa $m^{1/2}$) and Morales et al. [9] (1.3–1.5 MPa $m^{1/2}$). On the other hand, K_{IC} for LWO is similar to that reported for YSZ electrolytes [9].

Table 2
Estimation of K_{IC} for LWO56 with different sintering temperatures.

Composition	$T_{sintering}$ (°C)	Grain size (µm)	K_{IC} (MPa $m^{1/2}$)
LWO56	1400	∼1–3	1.9 ± 0.1
	1500	∼3–10	2.1 ± 0.2

4. Conclusions

Nanoindentation has been employed in order to extract the mechanical properties of a new material to be used as proton conducting electrolyte or membrane material for gas separation. The hardness without strain gradient plasticity contribution and Young's modulus were determined to be ∼8–9 GPa and ∼130 ± 15 GPa, respectively. The experimental results suggest that neither the hardness nor the Young's modulus are affected by the sintering temperature or the composition, so that slight non-stoichiometry within the studied range does not pose a problem from the mechanical properties point of view.

Fracture toughness has been calculated to be ∼2 MPa $m^{1/2}$ for LWO56. The experimental results suggest that LWO presents sufficient mechanical characteristics to be used in the mentioned high temperature devices. Also, we have shown that the model from Nix and Gao provides an excellent description of the dependence of the hardness with penetration depth in lanthanum tungstate ceramic materials.

Acknowledgements

The authors would like to thank the Serveis Cientificotècnics (SCT, University of Barcelona) for the AFM data (SCT, University of Barcelona) and the Spanish MCTE under Project MAT2008-06785-C02-01 by the financial support. Support from ''Ministerio de Educación y Ciencia'' for funding through the program MAT2004-03856 and the NANOMAT ''nanoPCFC'' project (182090/510) from Dr. Magrasó are gratefully acknowledged.

References

[1] M. Yoshimura, J.F. Baumard, Electrical conductivity of solid solutions in the system cerium oxide-lanthanum tungsten oxide (CeO_2–La_6WO_{12}), Mater. Res. Bull. 10 (1975) 983–988.
[2] T. Shimura, S. Fujimoto, H. Iwahara, Proton conduction in non-perovskite-type oxides at elevated temperatures, Solid State Ionics 143 (2001) 117–123.
[3] R. Haugsrud, Defects and transport properties in Ln_6WO_{12} (Ln = La, Nd, Gd, Er), Solid State Ionics 178 (2007) 550–560.

[4] R. Haugsrud, K. Kjølseth, Effects of protons and acceptor substitution on the electrical conductivity of La_6WO_{12}, J. Phys. Chem. Solids 69 (7) (2008) 1758–1765.
[5] W. Oliver, G. Pharr, Measurement of hardness and elastic modulus by instrumented indentation: advances in understanding and refinements to methodology, Journal of Materials Research 19 (1) (2004) 3–20.
[6] J.J. Roa, X.G. Capdevila, M. Martínez, F. Espiell, M. Segarra, Nanohardness and Young's modulus of YBCO samples textured by the Bridgman technique, Nanotechnology (2007), 18 385701/1-385701/6.
[7] A.C. Fischer-Cripps, Nanoindentation, Springer, New York, 2002.
[8] A. Magrasó, C. Frontera, D. Marrero-López, P. Núñez, New crystal structure and characterization of lanthanum tungstate "La_6WO_{12}" prepared by freeze-drying synthesis, Dalton Trans. 46 (2009) 10273–10283.
[9] M. Morales M., J.J. Roa, X.G. Capdevila, M. Segarra, S. Piñol, Mechanical properties at nanometric scale of GDC and YSZ used as electrolyte for SOFCs, Acta Mater. 58 (7) (2010) 2504–2509.
[10] R. Haugsrud, T. Norby, Proton conduction in rare-earth ortho-niobates and ortho-tantales, Nat. Mater. 5 (2006) 193–196.
[11] E. Jiménez-Piqué, Y. Gaillard, M. Anglada, Instrumented indentation of layered ceramic materials, Key Eng. Mater. 333 (2007) 107, pp. 107.
[12] I. Horcas, R. Fernández, J.M. Gómez-Rodríguez, J. Colchero, J. Gómez-Herrero, A.M. Baro, WSXM: a software for scanning probe microscopy and a tool for nanotechnology, Rev. Sci. Instrum. (2007), 78 013705/1-013705/8.
[13] T.L. Anderson, Fracture Mechanics: Fundamentals and Applications, Taylor & Francis, 2005, , ISBN: 978-0-8493-1656-2.
[14] B.R. Lawn, A.G. Evans, D.B. Marshall, Elastic/plastic indentation damage in ceramics: the median/radial crack system, J. Am. Ceram. Soc. 63 (1980) 574.
[15] M. Laugier, Load bearing capacity of TiN coated WC–Co cemented carbides, J. Mater. Sci. Lett. 2 (1983) 419–421.
[16] R.D. Dukino, M.V. Swain, Comparative measurement of indentation fracture toughness with Berkovich and Vickers indenter, J. Am. Ceram. Soc. 75 (1992) 3299–3304.
[17] D. Casellas, J. Caro, S. Molas, J.M. Prado, I. Valls, Fracture toughness of carbides in tool steels evaluated by nanoindentation, Acta Mater. 55 (2007) 4277.
[18] M. Kaji, M.E. Stevenson, R.C. Bradt, Knoop microhardness anisotropy and the indentation size effect on the basal plane of single-crystal alumina (sapphire), J. Am. Ceram. Soc. 85 (2) (2004) 415–422.
[19] V. Menvie Bekale, G. Sattonnay, C. Legros, A.M. Huntz, S. Poissonnet, L. Thomé, Mechanical properties of cubic zirconia irradiated with swift heavy ions, J. Nucl. Mater. 384 (2009) 70–76.
[20] T. Mokkelbost, H.L. Lein, P.E. Vullum, R. Holmestad, T. Grande, M.A. Einarsrud, Thermal and mechanical properties of $LaNbO_4$-based ceramics, Ceram. Int. 35 (2009) 2877–2883.
[21] W.C. Oliver, G.M. Pharr, An improved technique for determining hardness and elastic modulus using load and displacement sensing indentation experiments, J. Mater. Res. 7 (1992) 1564.
[22] R.F. Cook, G.M. Pharr, Direct observation and analysis of indentation cracking in glasses and ceramics, J. Am. Ceram. Soc. 73 (4) (1990) 787–817.
[23] K. Sato, H. Yugami, T. Hashida, Effect of rare-earth oxides on fracture properties of ceria ceramics, J. Mater. Sci. 39 (2004) 5765–5770.